An updated version of the SZ-plugin: from space to space-time data-driven modeling in QGIS

Giacomo Titti[1*], Liwei Hu[1], Pietro Festi[1], Letizia Elia[3], Lisa Borgatti[1], Luigi Lombardo[2]

Abstract

The geospatial community usually makes use of GIS environments to handle databases and pre-process their information. Actual analyses, especially data-driven ones, are performed outside GIS platforms. This interrupts the flow of information and the processing chain in a number of I/O operations that inevitably slow down the overall analytical protocols. The first version of the SZ-plugin attempted to mitigate this issue by offering a modeling solution from within QGIS. However, the available models in the SZ-plugin essentially boiled down to binary classifiers, whose dimensionality was constrained to address pure spatial problems. In this updated version, we focused on two major aspects: *1*) a space-time extension and *2*) the inclusion of a regression option in addition to the already existing classification one. These two aspects have been introduced as part of two new models, namely, a Generalized Additive Modeling and a Multi-Layer Perceptron. In short, these would allow users to obtain susceptibility and intensity estimates in space and time. An improved graphical reporting tool has also been implemented. This makes it possible to produce relevant statistical summaries as well as cartographic outputs for users to directly integrate into their technical reports or scientific documents. The problem of landslide prediction is taken as a reference in Taiwan, but the same plugin can be used to perform regressions or classifications for any other phenomenon associated with (e.g.) digital soil mapping, wildfire and gully erosion modeling, land-use or tree species detection, etc.

Keywords: SZ-plugin; QGIS; Data-driven modeling; Space-time classification and regression; Open-source.

[1]Department of Civil Chemical Environmental and Materials Engineering, Alma Mater Studiorum University of Bologna, Viale Risorgimento, 2, 40136, Bologna, Italy

[2]University of Twente, Faculty of Geo-Information Science and Earth Observation (ITC), PO Box 217, Enschede, AE 7500, Netherlands

[3]Istituto Nazionale di Geofisica e Vulcanologia, Sezione di Bologna, Bologna, Viale Berti Pichat 6/2, 40127, Bologna (BO)

1 Introduction

The notion of susceptibility modeling covers multiple areas in geoscience. The general definition boils down to the probabilistic assessment of locations where a given process may take place driven by geo-environmental factors. Even in the case of landslide science, the spatial nature of most applications stems from the historical evolution of the susceptibility concept. The first digital record of a susceptibility assessment dates back to Brabb et al. (1972). There, Earl Brabb's expert opinion dictated the description of the landscape under consideration into slopes labeled with a different level of proneness to failure. Since then, the susceptibility literature has significantly evolved, with a number of milestones to be mentioned to understand the current state-of-the-art. One of the most critical milestones is likely the contribution by Varnes and the IAEG Commission on Landslides and Other Mass-Movements (1984), where the authors disentangled the landslide prediction theme into three components. The first corresponds to predicting locations where landslides occur; the second represents the onset of the occurrence, either expressed precisely when or how frequently, while the third consists of the level of threat associated with a given mass movement or population. This notion was further refined by (Guzzetti et al., 1999) into a specific analytical protocol for each of the components above, with slight variations to the hazard definition itself.

These moments mark the definition of a standard, whose implementation in international guidelines (Fell et al., 2008) consolidated the idea that the spatial component of the landslide prediction should be treated separately from the temporal one. In turn, this implied that the susceptibility, or spatial probability of landslide occurrence, has been interpreted as a temporally-invariant characteristic of any landscape (see, Steger and Kofler, 2019).

However, this is obviously not the case in reality, nor should it be modeled in such a way. Some landscape characteristics could be considered static. To this class belong geological features, whose variations manifest on temporal scales far longer than the modeling requirements. Additionally, one could assume that in most cases, topographic changes cannot be captured through Digital Elevation Model data because it is not possible to obtain terrain models regularly unless repeated and consistent investments are made for surveying and/or processing relevant data. Thus, terrain characteristics are often assumed to be time-invariant as well. On the other side of the spectrum, the landslide triggers or predisposing factors act on much shorter timescales, from seconds to minutes in case of earthquakes and from hours to days in case of rainfall events. In between the extremes of this temporal spectrum, some landscape processes act at an intermediate level, with land use changes being responsible for modifying the landslide susceptibility on a monthly to yearly basis. Similarly, wildfires are processes known for elevating the susceptibility up to three years, through a mechanism where the heat generated by burning biomass alters the physical characteristics of the shallow soil column. Aside from the high temperatures generated by fires, even regular temperature variations control hydrological (Ray et al., 2010) and geotechnical (Loche and Scaringi, 2023) soil characteristics, over a temporal range expressed sub-daily (Melis et al., 2020) to yearly

(Loche et al., 2022). Anthropic activities may also contribute to relatively rapid susceptibility changes, especially road constructions (Forte et al., 2021), with instabilities even observed within a year from the slope cut (Tanyaş et al., 2022).

This is to highlight that there is no such thing as a static landscape and, thus, neither is nor should be the susceptibility. This is especially valid across active landscapes continuously shaped by weathering agents, tectonic and climatic stresses, as well as earth's surface processes in general. This is enhanced by the extreme agents under climate change conditions.

As a result, the need to decouple the "static" nature of the landslide occurrence probability from the "temporal" component mostly arose, at the time of the inception of the concept, from the limited capacity to capture and express dynamic landscape processes. This need becomes even more evident when considering the limited modeling capabilities until the 1990'ies. In other words, not only was it prohibitive to capture landscape dynamics, but it was equally hard to define a modeling paradigm able to estimate them.

This situation essentially stayed the same throughout the years, even when data and computational power would allow one to estimate susceptibility both in space and time. For instance, a number of recent examples still compute the susceptibility independently from rainfall thresholds and then combine the respective results (Lee et al., 2016; Segoni et al., 2015, 2018b). This is also why several codes, plugins and software meant to automatize the susceptibility assessment procedure have been conceived to address purely spatial classification tasks. To this category and from the oldest to the newest belong *MamLand* (Akgun et al., 2012), *GeoFIS* (Osna et al., 2014), *LAND-SE* (Rossi and Reichenbach, 2016), the *LSM* module for Netcad Architect (Sezer et al., 2017), *r.landslide* (Bragagnolo et al., 2020), *LSM Tool Pack* (Sahin et al., 2020), *LSAT PM* (Torizin et al., 2022), *PyLandslide* (Basheer and Oommen, 2024).

Following the same trend, the first version of the SZ-plugin (Titti et al., 2022) aimed at offering a plugin for spatial susceptibility modeling within the most used open-source GIS platform, i.e. QGIS (Flenniken et al., 2020). The idea is that by calling a susceptibility modeling workflow directly from QGIS, one would bypass all the input/output operations that typically affect the procedure. For instance, one typically maps landslides in GIS, and in the same platform, raster and vector operations are carried out to create a data matrix. The same matrix is then exported and imported into computing platforms such as R (Crawley, 2012), Python (Van Rossum et al., 2007), Octave (Eaton et al., 1997) etc., where the actual classification is performed, only to export the results once more which is then called from GIS for addressing scientific illustration needs. The SZ-plugin allows the user to run all those processes in one, user-friendly platform without the necessity to write code lines because of the Graphical User Interface available (see also the application in Titti et al., 2024).

In the literature, the "static" nature of the susceptibility has been challenged on several occasions (e.g., Reichenbach et al., 2014). The work of Samia et al. (2017a) and Samia et al. (2017b) started looking into how to move past pure spatial modeling. The authors achieved

this by proposing a sequential and simplified solution where the static predictors typical of susceptibility models were combined with the information on landslide presence/absence that occurred prior to the modeled landslide period. The same experiment was later explored and extended for the same area by Lombardo et al. (2020), marking the introduction of the first space-time landslide predictive model. This model architecture would simultaneously treat space and time. However, the information provided by traditional static predictors was combined with that of two explanatory variables acting at a latent level, one to control the interdependence between adjacent mapping units and one to control the interdependence between adjacent temporal units. In other words, no direct information on predictors acting at a relatively fast temporal scale was still included. This is the case for Wang et al. (2022) and Ahmed et al. (2023), where the authors combined static and dynamic covariates to estimate annual variations of susceptibility. This direction has opened up for analogous space-time experiments, where the considered *1*) mapping units were upscaled to Slope Units (SUs) (Fang et al., 2024b) and grid-cells (Steger et al., 2023), and *2*) temporal units were upscaled from years (Wang et al., 2024) to days (Moreno et al., 2024).

The present contribution further adds to the current literature by developing a suite for data-driven space-time modeling, implemented in an updated version of the SZ-plugin. Details on the new version of the plugin will be provided in the remainder of the manuscript, focusing not specifically on the experimental design and related performance but rather on the modeling capabilities the new SZ-plugin has to offer.

2 Test site

To showcase the space-time modeling extension of the SZ-plugin, we used the annual partition in SUs of Taiwan already appeared in Fang et al. (2024a). These SUs have been generated with the latest version of the *r.slopeunits* software made by Alvioli et al. (2016), in which flat areas can be directly removed from the calculation to avoid including trivial terrain information in the susceptibility model (Steger and Glade, 2017).

The resulting spatial partition totaled 645036 SUs across the whole space-time domain. This translates into 46074 individual SUs partitioning Taiwan, and repeated 14 times, one for each year under consideration between 2004 and 2018. Each of these polygons contains a yearly description of *1*) landslide presence/absence labels to support a dynamic susceptibility assessment (as per Steger et al., 2024), *2*) landslide planimetric areas to support a dynamic landslide extension assessment (as per Lombardo et al., 2021), and *3*) also reports relevant predictors to support data-driven modeling routines. Notably, the landslide type mostly corresponds to shallow debris slides and flows.

Figure 1 indicates the test site and maps the landslide area information over more than a decade. The temporal aspects of landslide occurrences and (log) planimetric area per SUs are shown in the respective panels on the right. Notably, the dates do not refer to a specific year but rather to two subsequent ones. This is due to the acquisition dates of the remote

scenes used to support the landslide mapping procedure. In fact, they are representative of the period between August 1 of a given year and July 31 of the following one. This makes the overall surveyed period 12 months long while spanning over two years.

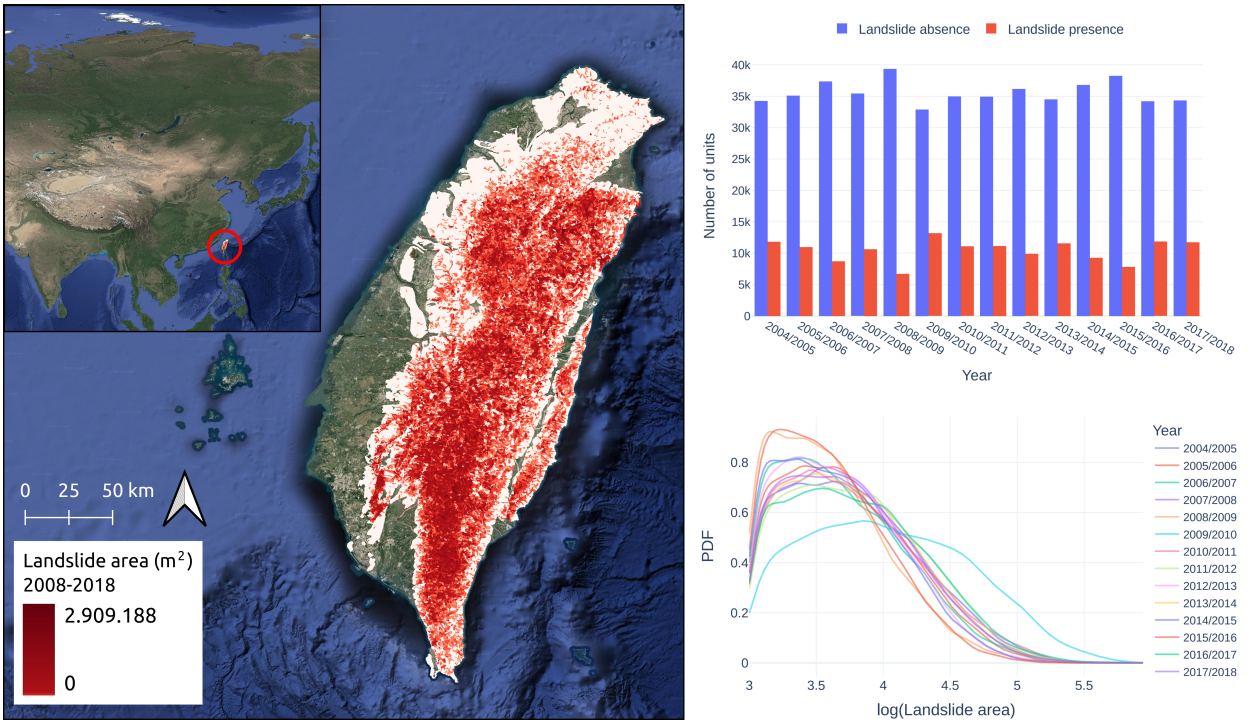

Figure 1: Overview of the study area. The temporal dimension of the landslide area had been compressed purely in space for simplicity. White areas correspond to the mask where the topography is not flat. As for the red colorbar, it shows the landslide area aggregated per individual SUs as the sum over the period between 2004 and 2018. The barplot to the right presents an overview of the landslide presence/absence distribution aggregated for each year. The bottom panel offers the same temporal view of the landslide area information expressed logarithmically.

3 Material and methods

This section offers an overview of the modeling extensions implemented in the new version of the SZ-plugin for QGIS. In total three modules are available: the first one is the space-time adaptation of the module already implemented in the previous version of the SZ-plugin which includes Decision Tree, Support Vector Machine and Random Forest algorithms. The second one corresponds to a space-time Generalized Additive Model (GAM) implementation to solve for binomial and Gaussian likelihoods. As for the second modeling archetype, the SZ-plugin now offers an option for running basic spatiotemporal Neural Networks both in classification and regression modes.

The second and third options will be elaborated below on Taiwan case study, keeping

in mind that the space-time classification options are meant to support dynamic susceptibility modeling, whereas the space-time regression options addresses the same for intensity modeling. Therefore, a comparison between dynamic modeling of *1)* susceptibility, which corresponds to the probability of occurrence of a given phenomenon, and *2)* intensity, which indicates the level of threat associated with it, have been performed. Finally, *3)* a space-time prediction has been reported.

The examples will be centered around landslides, but we stress that the same can be done for any hazard or other phenomena distributed in space and time, such as: wildfires, gullies, but also other fields of geospatial application typically associated to digital soil mapping, land use and tree species detection, etc..

3.1 Space-time GAM

By calling Y the random variable indicating how likely the mapping unit is susceptible to landslides, let $\boldsymbol{X} := (X_1, .., X_p)$ be the set of predisposing factors; GAMs assume that the probability of a mapping unit being susceptible conditional on the predisposing factors $\mu := \mathbb{E}[Y|\boldsymbol{X}]$ is related to the independent variables via a *link* function g

$$g(\mu) = \alpha + \sum_{j=1}^{p} f_j(X_j), \tag{1}$$

where α is the global intercept, each f_j the unknown smooth function expressing the linear or nonlinear relationship between the j-th predisposing factor X_j and the response variable Y.

3.1.1 Binomial likelihood

We recall that international guidelines on landslide hazard require estimating how prone a given landscape may be to generating slope failures (Fell et al., 2008). The numerical translation of this definition involves a response variable Y assumed to behave according to a Bernoulli distribution

$$Y \sim \text{Bernoulli}(\mu). \tag{2}$$

This implies that either the mapping unit is susceptible, denoted with probability $\mu \in [0, 1]$ or that it is not, with a probability $1 - \mu$.

In this case, a commonly used link function is the logit link:

$$g(\mu) = \log\left(\frac{\mu}{1-\mu}\right). \tag{3}$$

The GAM model with smooth functions f_j to be estimated is:

$$\log\left(\frac{\mu}{1-\mu}\right) = \alpha + \sum_{j=1}^{p} f_j(X_j), \tag{4}$$

equipped with a Binomial error distribution. Going back to placing such models in the context of international guidelines, space-time binomial GAM generate outputs which fall in a grey area. In fact, the standard notion of landslide hazard requires three components to be estimated (separately). The former is the susceptibility, traditionally considered to be a static characteristic of any landscape under consideration. As for temporal probability aspects, these are usually determined as the return period of the main landslide trigger or as the occurrence period. Space-time binomial GAM fundamentally addresses both requirements in a single modeling archetype, allowing the computed probabilities to contextually vary across any mapping and temporal units of choice.

3.1.2 Gaussian likelihood

We also implemented an alternative probability distribution to model continuous response variables. This corresponds to the Gaussian case, defined with mean $\mu \in \mathbb{R}$ and variance σ^2

$$Y \sim \mathcal{N}(\mu, \sigma^2), \tag{5}$$

Differently from the binomial likelihood, the GAM here uses the identity link function,

$$\mu = \alpha + \sum_{j=1}^{p} f_j(X_j) \tag{6}$$

with a Normal error distribution. To provide some context on how this likelihood can be used in the context of landslide modeling, we recall here that landslide are commonly mapped as polygons. Therefore, each landslide is associated with the information of its planimetric extent. Due to the heavy-tailed nature of the landslide area distribution, one has two options to model landslide intensity. The first option, also the one we followed here, is to transform the landslide areas into their logarithm. Because this transformation symmetrically distributes the range of landslide areas over the logarithmic scale, it is then possible to adopt a Gaussian likelihood to regress this quantity against the selected set of covariates.

A valid but more complex alternative could have been implementing various likelihoods inspired to extreme value theory. However, because we scripted this plugin with the idea of making it usable beyond the landslide context and because the Gaussian distribution is the most common case, we avoided the option for statistics of extremes (yet laid out plans in this direction for a subsequent release).

We stress here that if one would include mapping units with no landslides in the landslide area model, most of the space-time dataset would have areas equal to zero. This would create a number of technical complications discussed at length in Lombardo et al. (2021). To avoid them, we only extract the positive range of landslide area values and take their logarithm. The complementary dataset will then be used to generate predictions over it. To follow up on the considerations related to international guidelines, we recall once more that the

landslide hazard definition also includes a third term referred to as intensity (Bryce et al., 2022). This reflects the level of threat associate with a landslide and, for regional models, it has been mostly estimated as a function of the landslide planimetric area, hence the use of the Gaussian likelihood implemented here.

3.2 Space-time Multi-Layer Perceptron

Although space-time generalized additive models are able to model possible nonlinear relationships between every single predictor X_j and the response variable Y by generalizing the regression coefficients with generic smooth functions f_j , an additive scheme is still assumed in the right-hand side term of Eq. (1). An alternative way to approach the problem of landslide susceptibility mapping is to learn from data not only the distribution of training dataset, i.e. realizations of Y and X_j,just as in the standard procedure to find the unknown smooth function f_j and S in the space-time GAMs, but also the relationship itself between the predictors and the response variable. Formally, we would like to find an implicit parametric function $\nu_{\boldsymbol{\Theta}}$ defined on the space of predictors which outputs the likeliness of a mapping unit to be a susceptible zone:

$$\nu_{\boldsymbol{\Theta}} : \mathbb{R}^p_{\boldsymbol{X}} \to \mathbb{R}_Y, \tag{7}$$

where $\boldsymbol{\Theta}$, the set of all parameters of this function, encodes both the information on the statistical model for the variables and the probability distribution of these variables. This is basically the idea behind the simplest of all artificial Neural Networks (NNs), known as Multi-Layer Perceptron (MLP).

Artificial Neural Networks form a model of computation inspired by human brain structure with goals to perform high-complexity level tasks. General NNs consist of many processing units called *neurons* that interact using weighted connections (Hinton, 1989). Each neuron has a *state* which is determined by input received from other *neurons* in the network. More precisely, the neuron collects the total input, and, through an activation function, it might change its state accordingly. This is the reason why the *state* of a neuron is also called its activity level.

MLP is a multilayer feed-forward NN architecture (Rumelhart et al., 1986; LeCun et al., 2015), meaning that the flow of information is unidirectional along fixed-sized groups of *neurons*. Each group of *neurons* is called a layer, due to the schematic graph representations particularly popular of NNs. No connections are present within a layer or from higher to lower layers, by adopting the convention of having the input at the bottom and the output on the top in this representation. Furthermore, a MLP is fully connected meaning that the state of each *neuron* of every layer depends on states of all *neurons* in the previous layer.

In mathematical terms, given an input vector $(x_1, \ldots, x_p) \in \mathbb{R}^p$, the state of each *neuron* in the input layer of a MLP, which has number of *neurons* equal to p, is just a copy of the values of this vector, simulating the intensities of signals the brain can receive from sensory organs. If we denote the state of a *neuron* in the first hidden layer as $z^{(1)}$, then

$$z^{(1)} = h^{(1)}\left(b^{(1)} + \sum_{j=0}^{p} w_j^{(1)} x_j\right), \tag{8}$$

where $w_j^{(1)}$ denotes the weight of the connection with the j-th *neuron* from the input layer, $b^{(1)}$ a bias term, and $h^{(1)}$ a nonlinear activation function. We note that the bias term is related to the threshold of the *neuron* (Hinton, 1989). The same expression can be generalized for the i-th *neuron* in the generic k-th layer, with $k \geq 2$ and $i = 1, \ldots, n_k$, where n_k is the number of *neurons* of k-th layer:

$$z_i^{(k)} = h_i^{(k)}\left(b_i^{(k)} + \sum_{j=1}^{n_{k-1}} w_{ij}^{(k)} z_j^{(k-1)}\right). \tag{9}$$

The number $w_{ij}^{(k)}$ is the weight of the connection between the i-th *neuron* in the k-th layer and the j-th *neuron* from the $(k-1)$-th layer.

If K is the number of hidden layers of the MLP, the likeliness of the mapping unit to be a susceptible zone is given by the state of the output layer, consisting of one single *neuron*, with value $z_1^{(K+1)}$.

A common choice of nonlinear activation functions for hidden layers is the rectified linear unit (ReLU):

$$\mathrm{ReLU}(a) = \max(0, a). \tag{10}$$

Activation functions in a MLP typically do not have any learnable parameters, therefore $\boldsymbol{\Theta}$ the set all learnable parameters in (7) consists of all weights and biases of *neurons* in the space-time MLP $\nu_{\boldsymbol{\Theta}}$ illustrated. In particular, the values of these learnable parameters are sought to minimize a loss function $\mathcal{L} = \mathcal{L}(\boldsymbol{\Theta})$ defined on the training dataset:

$$\boldsymbol{\Theta} \in \arg\min_{\boldsymbol{\theta}} \mathcal{L}(\boldsymbol{\theta}). \tag{11}$$

We observe that an MLP can be visualized as the composition of couples of linear-nonlinear functions corresponding to weights learning and activation functions. Therefore, it should not be surprising that the training process is carried out by means of the back-propagation algorithm introduced in Rumelhart et al. (1986), which is strictly related to the chain rule used for computing derivatives of composition of functions.

3.2.1 Classification task

The choice of the loss function is crucial to the predictive capability of the space-time MLP. Activation functions close to the output are related to the choice of the loss function. We just state that for the classification task, the space-time MLP implemented has as activation function of the output layer, the logistic function:

$$h(a) = \frac{1}{e^{-a} + 1}, \tag{12}$$

with a denoting the *pre-activation* value.

The loss function is chosen to be the binary cross-entropy, and for a single training sample

$$\mathcal{L}(y, p) = -(y \log(p) + (1 - y) \log(1 - p)), \tag{13}$$

where $y \in \{1, 0\}$ stands for the mapping unit to be a susceptible zone or not, respectively. While $p \in [0, 1]$ is the probability predicted by the space-time MLP $\nu_{\mathbf{\Theta}}$, in particular as the output of the above-mentioned logistic function.

3.2.2 Regression Task

As for regression problems, an identity activation function has been used. We observe that the choice of the identity is equivalent to remove the assumption that the output should be a probability as in the classification task. The associated loss function is the mean squared error, which for a single training sample has value:

$$\mathcal{L}(y, \hat{y}) = \frac{(\hat{y} - y)^2}{N}, \tag{14}$$

where $\hat{y}$ is the estimation given by MLP, and N is the number of training samples.

3.3 Performance metrics

The two available modes, classification and regression, require different metrics to be evaluated regarding their respective predictive performance. For this reason, we have equipped each mode, irrespective of the GAM or MLP context, with a suite of metrics automatically reported at the end of the fitting and cross-validation processes.

For the classification case, the SZ-plugin returns three parameters: Area Under the Curve (AUC), or the area under the Receiving Operative Characteristic (ROC) curve (Hosmer and Lemeshow, 2000), F1-score (Sokolova et al., 2006), and Cohen's Kappa (Ben-David, 2008). As for the regression mode, the SZ-plugin returns five parameters: Root Mean Square Error (RMSE) (Hodson, 2022), Mean Absolute Error (MAE) (Chai and Draxler, 2014), Mean Absolute Percentage Error (MAPE) (De Myttenaere et al., 2016), R^2 (Chicco et al., 2021) and Pearson Correlation Coefficient (Schober et al., 2018).

4 Results

This section offers an overview of all the accessible graphical output produced by the new version of the SZ-plugin.

4.1 Variable contribution

The first element of strength in statistical modeling has always been the ability to interpret the results, as opposed to the black-box machine learning tools. To put it simply, regression coefficients can always be visualized to understand the functional relations existing between dependent and independent variables. In the context of a GAM, the estimated relations have been mostly expressed nonlinearly through splines (Wood, 2004). The SZ-plugin also allows for estimating covariate effects as splines, but also as linear effect and categorical ones, as shown in Figure 2.

There, the effects belonging to the the space-time binomial calibration model are depicted in blue alongside the effects of the space-time Gaussian calibration model shown in red. We recall here that the binomial case should be interpreted as a model where landslide occurrence probabilities are estimates in space and time, as opposed to the Gaussian one, to be interpreted as a model where landslide areas are predicted instead.

Starting from the dataset published by Fang et al. (2024a) we selected a sub-group of covariates which includes: northness mean of SU (NorthM), eastness mean of SU (EastM), slope mean of SU (SlopeM), slope standard deviation of SU (SlopeStd), plan curvature mean of SU (PlanM), plan standard deviation of SU (PlanStd), profile curvature mean of SU (ProfileM), profile curvature standard deviation of SU (ProfileStd), maximum daily rain in the year averaged per SU (RainM), mean NDVI in the year averaged per SU (NDVIm), lithology (litho). The lithology of each SU is described by the main class present. The 15 classes of lithology are reported in Table 1.

id	Lithology
0	Alluvium
1	Andesite, basalt, and serpentine
2	Metamorphic limestone
3	Black schist, green schist, and sandy schist
4	Laterite, gravel, sand and clay
5	Mudstone intercalated with allochthon
6	Gneiss
7	Hard shale and sandstone
8	Agglomerate and tuffaceous sandstone
9	Sandstone, mudstone, and shale
10	Phyllite, slate, and sandstone
11	Sandstone, shale, and coaly shale
12	Quartzite, slate, and coaly shale
13	Shale, siltstone, and sandstone
14	Hard shale, slate, and Phyllite

Table 1: The identifiers used in the text for the 15 classes of lithology.

As for the effects shown in Figure 2, they should be read as follows: a negative value along the y-axis is diagnostic of a decrease in either the landslide occurrence probability or the

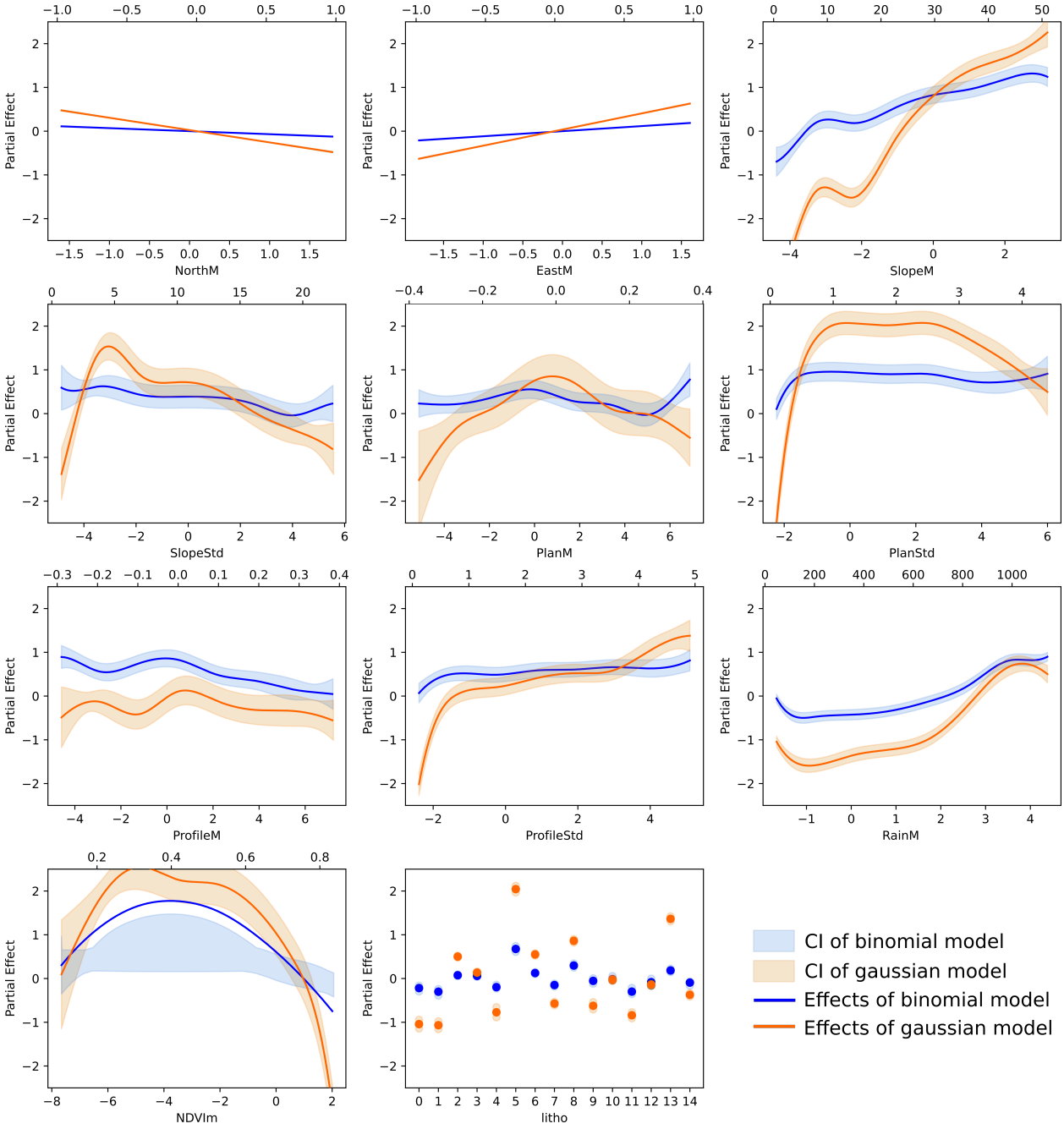

Figure 2: Covariate effects estimated for both the dynamic susceptibility (red colors) and intensity (blue colors) models.

estimated landslide area; a positive value instead is diagnostic of the opposite. To put things into perspective, it is interesting to see how the contribution of the mean steepness of a SU appears to be much more positive overall in the Gaussian case. Examining the two linear behaviors of Eastness and Northness, we also see some differences, with the former showing a negligible effect on the space-time susceptibility estimates, whereas the same covariate slightly contributes to decrease the estimated (log) landslide area northwards.

Ultimately, the categorical lithological effect is shown in the last panel, with certain lithologies also behaving slightly differently in between the two modeling options.

Another interesting aspect to highlight is that our plugin is now including a variable interaction option. We recall here that spline models are native solutions to estimate covariate effects. However, these can be implemented to estimate individual effects as well as the combined effect of two covariates. The latter option is commonly referred to as a variable interaction term (Opitz et al., 2022), and it is to be interpreted with the regression coefficient being estimated for the contextual values of two predictors at once. This modeling option is now also part of the SZ-plugin and an example of it is displayed in Figure 3.

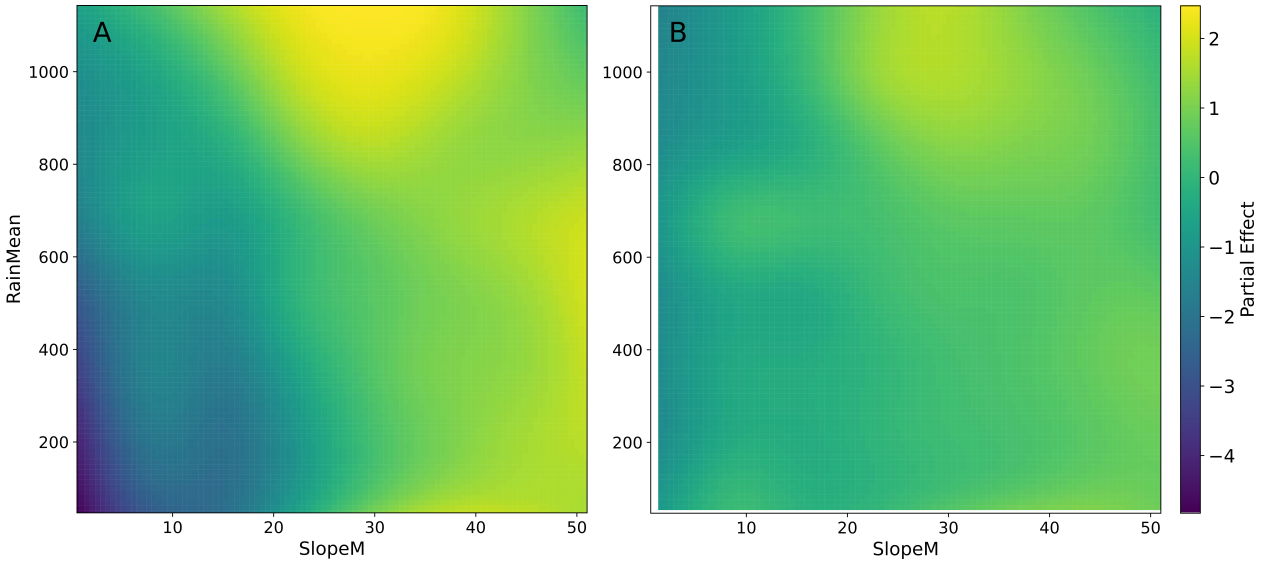

Figure 3: Interaction terms between mean slope steepness and yearly rainfall per SU shown in panel A for the binomial case and in panel B for the Gaussian one.

There, we plotted the interaction effect of the mean slope per SU together with the mean of maximum daily rainfall per year in each slope unit, this being shown both for the binomial and Gaussian cases. To provide a guide on interpreting these interaction effects, we can take the example of the susceptibility panel to the left (Figure 3A). There, SUs with mean slope steepness lower than 10 degrees and subjected to a mean rainfall lower than 600mm are marked with a strong negative regression coefficient. This contributes to lowering the probability that landslides are expected at those locations across the 14 years under consideration. Similarly, we can also interpret the interaction term estimated for the intensity case shown in the right panel (Figure 3B). There, SUs with mean steepness between

25 and 35 degrees exposed to mean rainfall amounts above 800mm are associated with very positive regression coefficients. This can be read with the expected landslide area (expressed in logarithmic scale) to be probabilistically higher than in any other conditions across Taiwan and across the examined period.

4.2 Dynamic Susceptibility

The additive structure of a GAM translates into combining the covariate effects shown in the previous section to produce a predictive equation, whose results, once transformed through the logit link are converted into probabilities. As our model is defined both over space and time, then the probabilities of landslide occurrence are assigned to each SU and to each year under consideration. Analogous considerations apply to the MLP classification case, which, once trained, estimates weights to each predictor that allow for generating pseudo-probabilities for any target SU.

This is also the mechanism behind cross-validation routines. The current version of the SZ-plugin allows users to automatically cross-validate in space, time, and space-time, both for the GAM and the MLP options. For the spatial case, we offer tow options: a random k-fold cross-validation method already present in the first version of the plugin and explained in Titti et al. (2022) and the same approach explained in Elia et al. (2023). There, a k-mean cluster analysis is run to group mapping units according to their location. In our case, we do so by clustering according to the latitude and longitude of the SU centroids. As a result, the SZ-plugin trains over all clusters but one, including temporal replicates, and then validates on the subset previously kept aside. The operation is iteratively repeated until all individual spatial subsets have been used to assess the prediction. In our analysis we generated 10 clusters, the results are shown in Figure 4. There, each ROC curve and its AUC are reported alongside the F1-score (F) and Cohen's Kappa (K) across ten spatial cross-validation subsets.

We have also implemented two versions of temporal cross-validation. The first one, called Leave One Out (LOO), iteratively excludes one year at a time from the training and uses it for predictive purposes. This would inevitably break the continuity of the temporal sequence. For instance, by excluding the year 2013, the model would be trained with all the SUs in the period between 2004 and 2012, plus all the SUs from 2014 to 2018. Therefore, to respect the consequentiality of the flow of time and the potential interdependence among landslide occurrences and predictor effects, we have also implemented a sequential cross-validation option called Time Series Split (TSS). This routine will train over one year and predict over the next in its first run. Then, in the second run, the training dataset would combine the first and second year to predict the third, and so on, until the sequence automatically reaches the last year (Figure 4).

Ultimately, the fourth panel of Figure 4 shows the spatiotemporal cross-validation option available in the SZ-plugin. This is essentially achieved by intersecting the spatial clusters generated with the k-mean based method with the LOO-time method. Therefore, in our

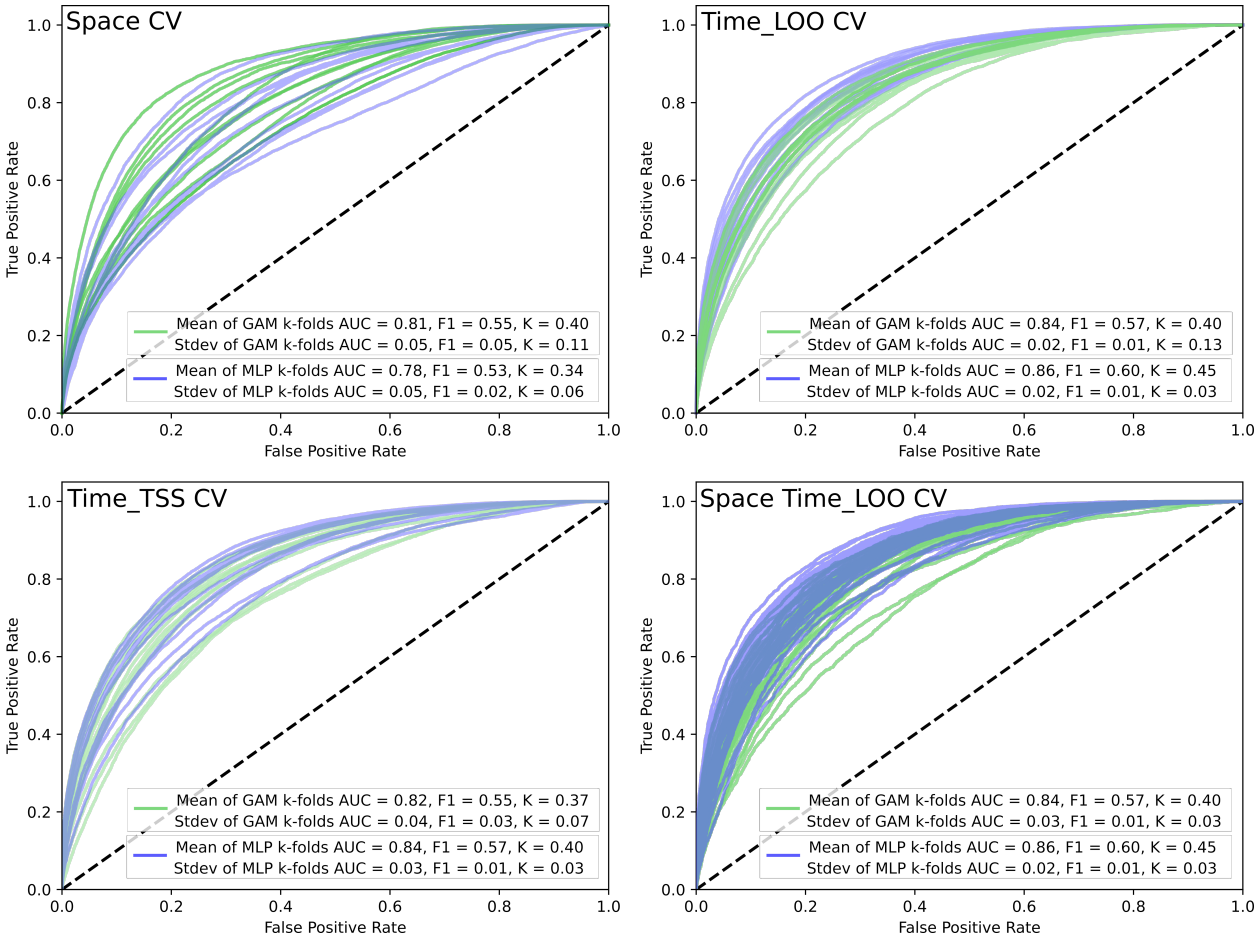

Figure 4: Cross-validation modes available for the GAM and MLP classifications in the new SZ-plugin release.

analysis, we intersected 3 spatial clusters together with the 14 years under study for a total of 42 space-time subsets. Similar to the previous examples, each of the 42 subsets is iteratively excluded until all of them are used for blind prediction.

To provide some interpretation, one can notice how the GAM option performs better than the MLP only for the spatial cross-validation case. As for the other three cross-validation modes, MLP slightly outperforms the GAM. This should not come as a surprise because machine learning tools such as MLP are known for their high performance. Conversely, GAM models are commonly known for their interpretability.

4.3 Dynamic intensity

Here, we offer an overview of the plugin's space-time modeling capabilities when selecting the regression mode. Similarly to the previous section, we have equipped the plug-in with the same cross-validations, with the option of using them to predict the log-landslide areas. To keep the same level of reporting capabilities we showed for the classification mode, we have implemented two performance assessment levels even in the regression case. To match the visualization provided before by the ROC curves, we graphically summarized the regression performance through QQ-plots (Figure 5).

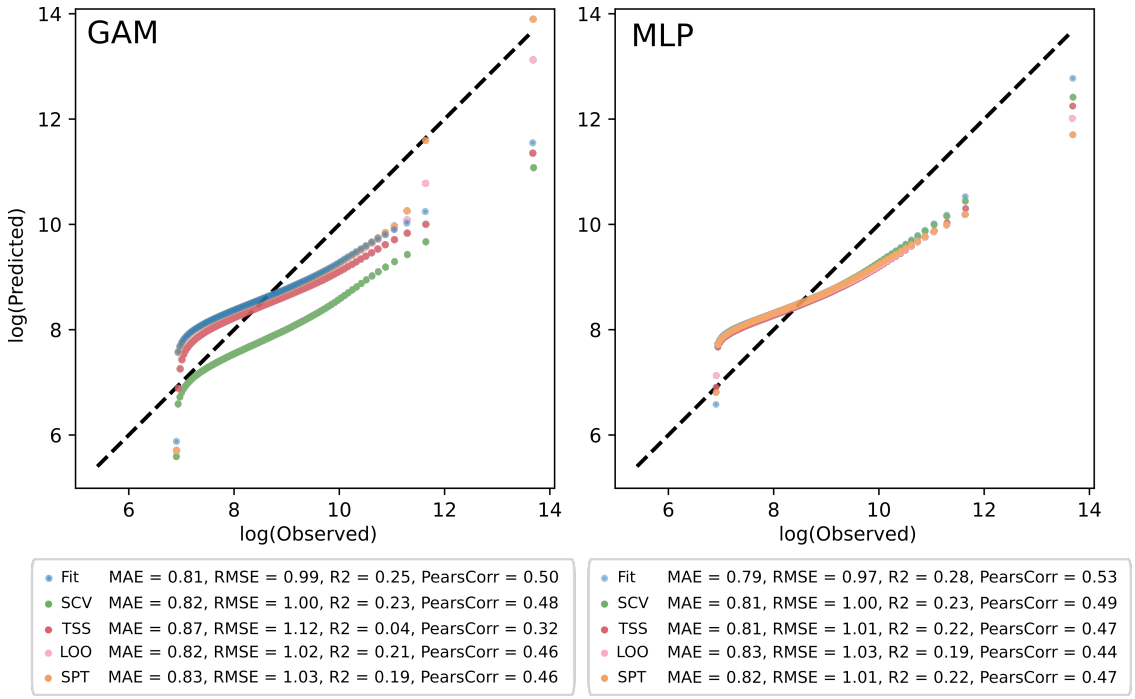

Figure 5: QQ-plots and associated model performance overview for the GAM and MLP modeling options.

These are built by taking the observed and predicted log-landslide area and plot their respective quantile distribution. An ideal model would reflect the distribution characteristics of the response variable, thus aligning each quantile couple along a 45-degree line.

Essentially, two vectors are needed to generate a QQ-plot, one for the response and one for the model output. In this case, we opted to maintain the same vector of observed data, where each element corresponds to a SU in space and time. The output of the fit naturally matches this dimensionality. However, the cross-validation routines intrinsically extract subsets. Therefore, the QQ-plots for the cross-validations are built by predicting over each excluded dataset and stitching these together again to match the size of the reference dataset. This procedure ensures that every quantile along the y-axis of Figure 5 is extracted from a distribution of log-landslide areas coming exclusively from SUs used for blind prediction.

To this graphical overview, we also added a series of numerical metrics to complete the evaluation. Notably, both the GAM and the MLP models are overestimating small landslide areas and underestimating large landslide areas. This is a typical characteristic of the Gaussian likelihood we used in the GAM case. Interestingly, though, it is also what stands out in the MLP panel. The main difference between the two panels is the variability associated with the two models, with the GAM showing significant variations across the cross-validation schemes. At the same time, the MLP outputs almost systematically overlap.

4.4 Landslide susceptibility and intensity mapping

Since its inception in the early 1970'ies (e.g., Brabb et al., 1972), susceptibility and hazard estimations required translating any assessment in map form. Despite the drastic changes in modeling options experienced since then, mapping is still the most important element to be addressed. For this reason, the new SZ-plugin release offers the option to translate the results of dynamic classification and regression results into maps. The way we thought of implementing this is for the SZ-plugin to access the model object where all regression coefficients (in case of a GAM choice) or all weights (in case of a MLP choice), and solve the predictive equation for any spatial object of interest. This offers the flexibility to map landslide susceptibility or log-landslide area predictions not only for the same data of the study site or time the given model has been trained with, but also to transfer the predictive function to other regions or times of interest. Moreover, this can be done for individual maps or by computing the summary statistics for multiple maps over time. Examples of such options can be found in Figure 6. There, we generated six susceptibility maps for the time interval between 2004 and 2018, three from the GAM and three from the MLP outputs. These correspond to the worst-case scenario over this period (the maximum of the annual probability per SU), the mean scenario, and the variability per mapping unit over the selected decade measured in a single standard deviation map.

The equivalent option is also available for mapping summary statistics of the landslide intensity. The results are shown in Figure 7. There, it is important to stress why we have kept the landslide area on a logarithmic scale. Taking the exponential to bring back the landslide area into its linear expression would imply exacerbating the errors we noticed for the left and right tail of the distribution (equivalent to the underestimation and overestimation discussed for Fig.5). Therefore, we keep rendering the geographic prediction as is, something

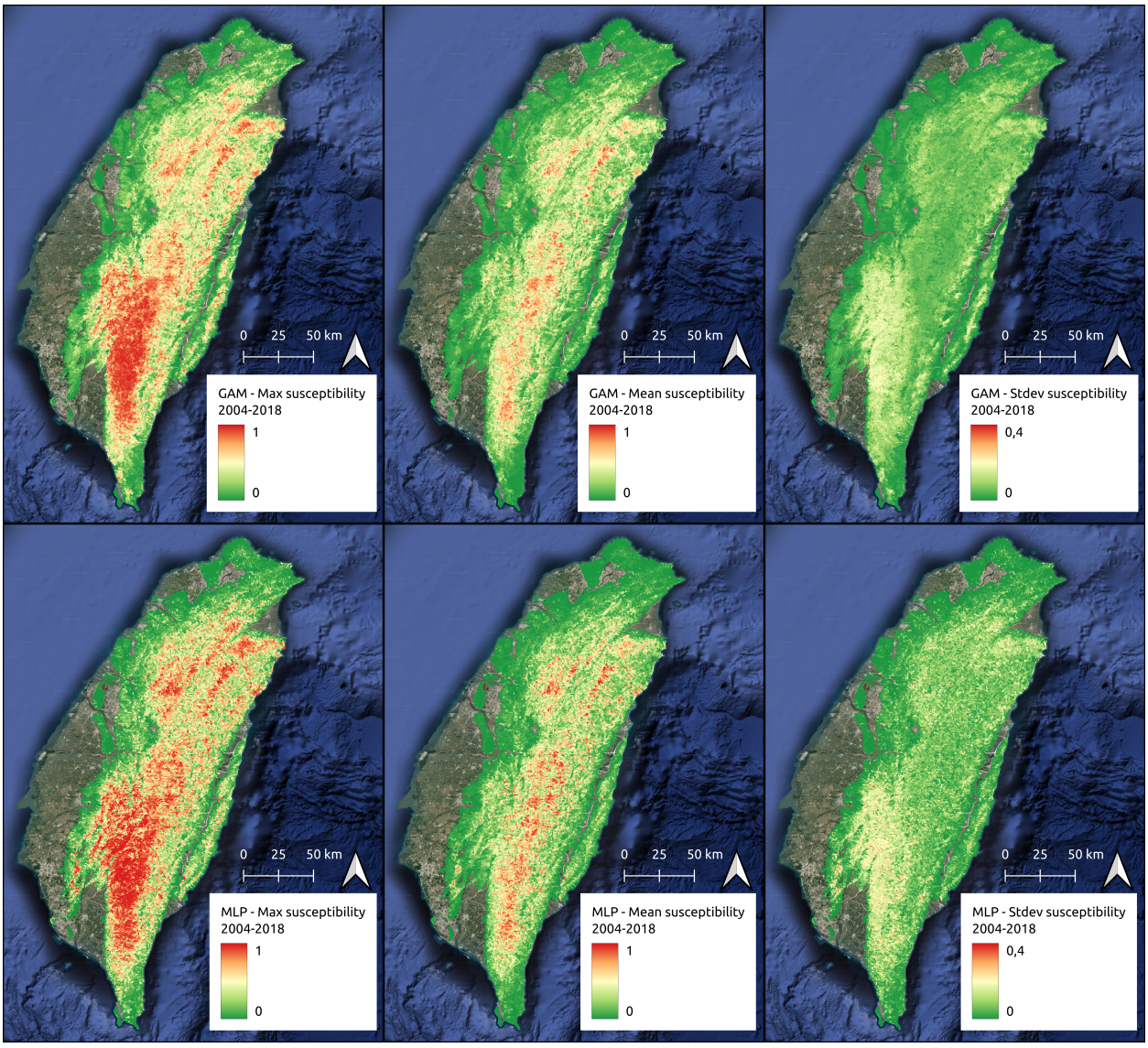

Figure 6: Examples of summary statistics (maximum, mean and standard deviation) of multiple susceptibility maps distributed between 2004 and 2018.

that can be justified thanks to the characteristic of the logarithmic function. In fact, the logarithm transformation is monotonic, which means that any landslide area that is smaller than another on the linear scale will also be smaller when transformed. In light of these considerations, the maps we show highlight where one could expect larger failures compared to other locations, over the 14-year period under consideration.

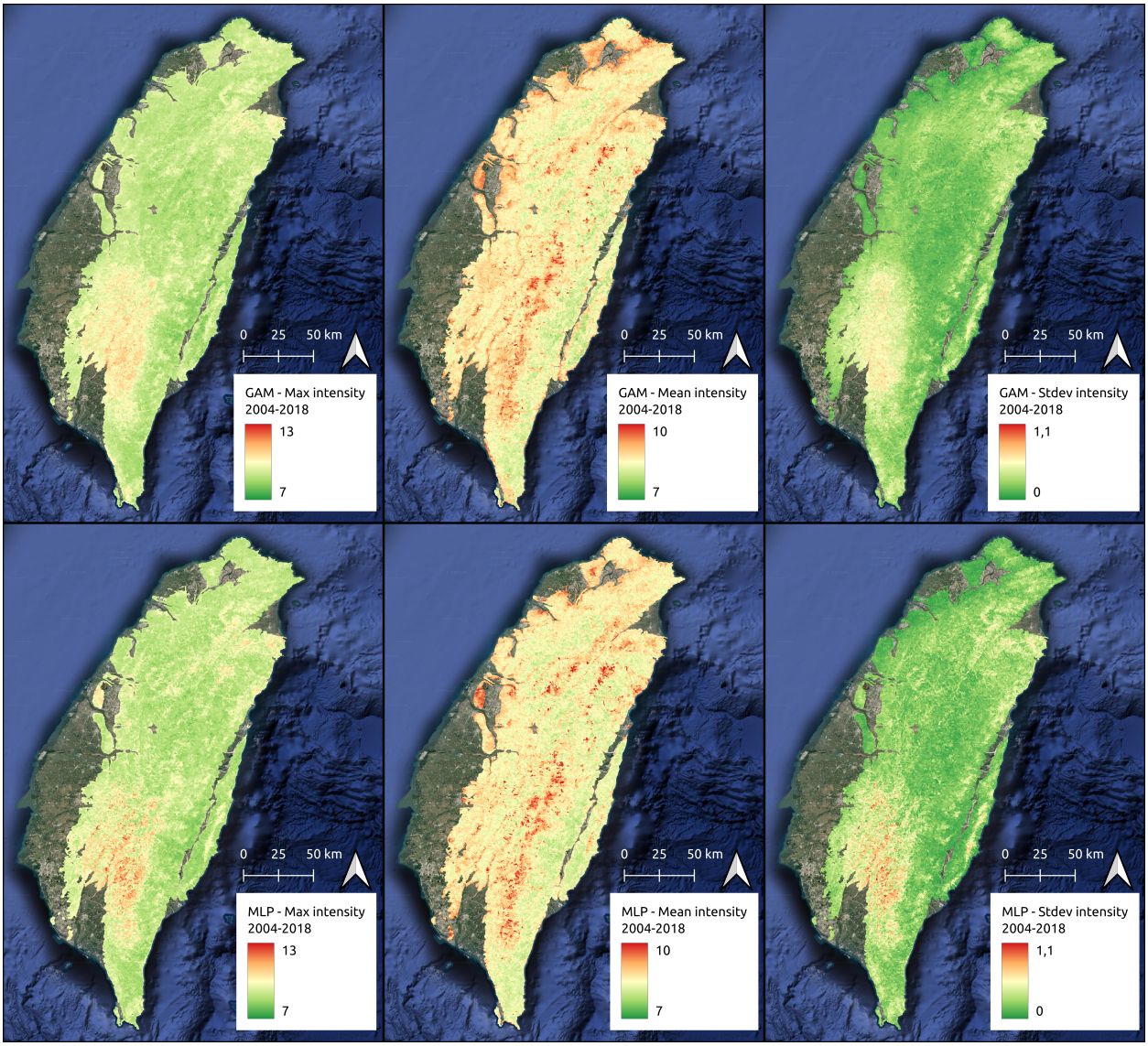

Figure 7: Examples of summary statistics (maximum, mean and standard deviation) of multiple intensity maps distributed between 2004 and 2018.

However, one may not necessarily be interested in plotting aggregated predictions over long periods but rather for specific years or temporal units. Figure 8 showcases four examples where, irrespective of the architecture of choice (GAM or MLP) or the model of choice (classification or regression), it is possible to generate individual maps. Therefore, we have generated GAM-based and MLP-based susceptibility and intensity maps for Taiwan, but

simulating for the period between August 1 2016 and July 31 2017. This only required populating the SUs with the relevant predictor set.

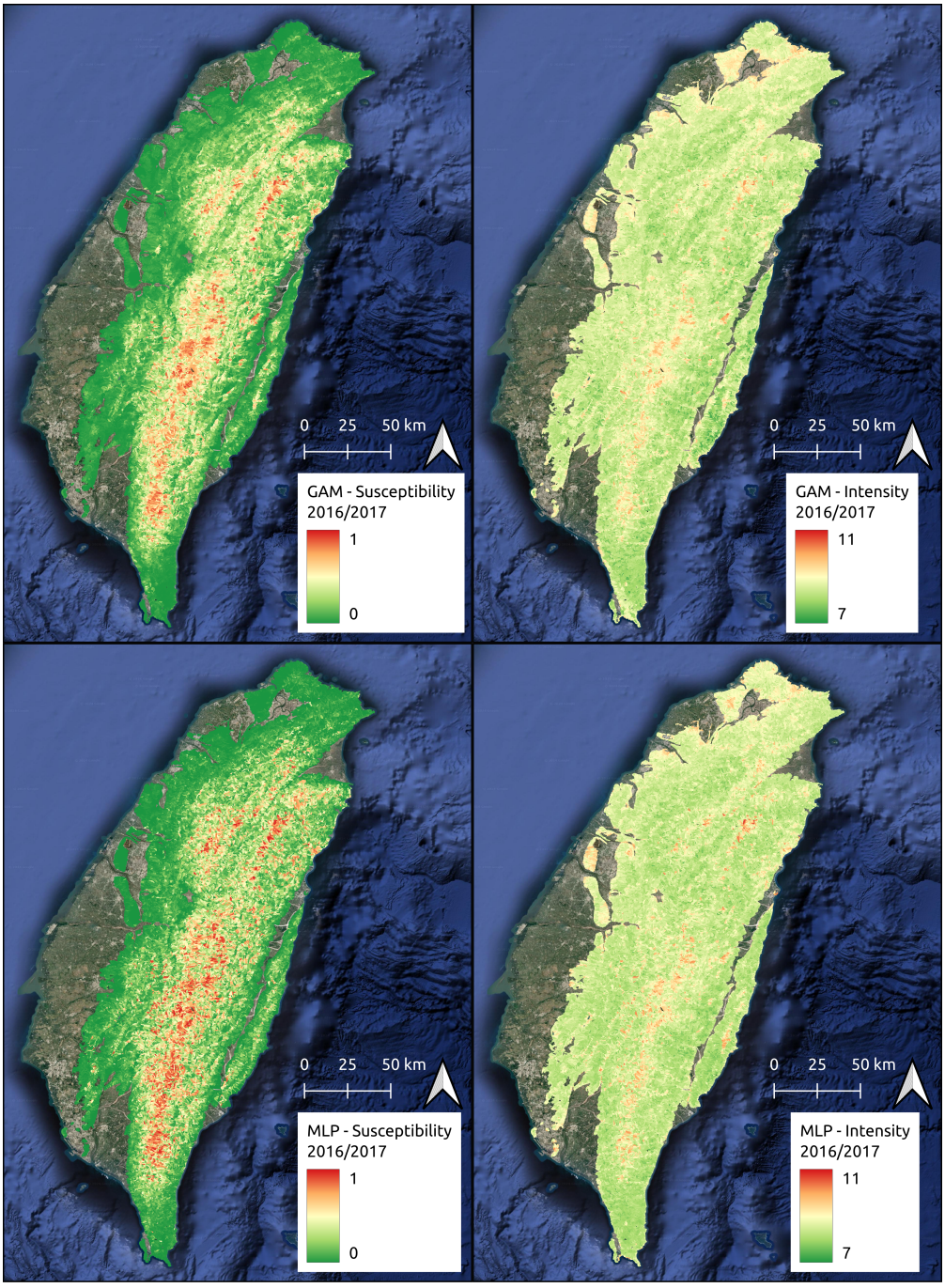

Figure 8: Simulations examples for a specific year (2016/2017) of interest involving susceptibility and intensity generated via both GAM and MLP options.

Ultimately, the same plotting capability is possible for data outside the domain of interest, whether this involves a different study area or time. In this case, we used the knowledge acquired from 2004 to 2018 to predict susceptibility and intensity in 2019 by updating,

temporary, the dynamic covariates selected.

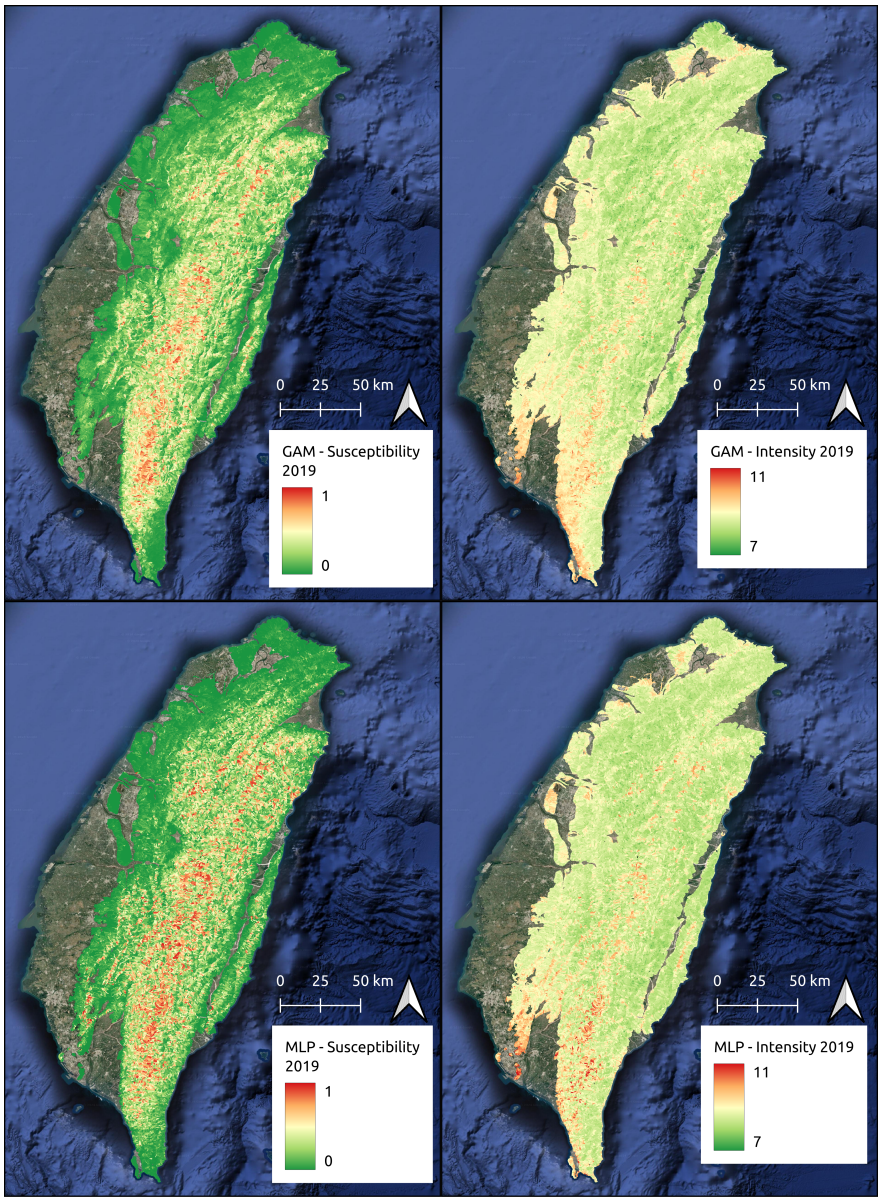

Figure 9: graphical example of the SZ-plugin used for simulation purposes outside the temporal domain (from the range 2004-2018 to 2019) the four models were originally built for. The same can be done simulating in another geographic area.

5 Discussion

More than fifty years of landslide data-driven modeling developments have led to two main outputs: i) one limited to static susceptibility analyses (Reichenbach et al., 2018) and ii) the other limited to rainfall thresholds (Segoni et al., 2018a).

However, current modeling capabilities offer much more than these two, mainly in the form of space-time models (Fang et al., 2024a). Moreover, almost the entirely of the data-driven literature has been confined to the estimation of occurrence probabilities, leaving aside how threatening landslides may be once triggered. These aspects belong to intensity data-driven efforts, also implementable as part of space-time models (Dahal et al., 2024b), and also in case of various natural phenomena (e.g., Millington, 2005; Barna et al., 2023). With these considerations in mind, we built the new version of the SZ-plugin, to offer anyone easy access to such modeling archetypes, specifically through the most common and open GIS platform.

A key requirement of any plugin is its usability. In this sense, we have equipped our tool with a straightforward graphical interface (see Fig. 10).

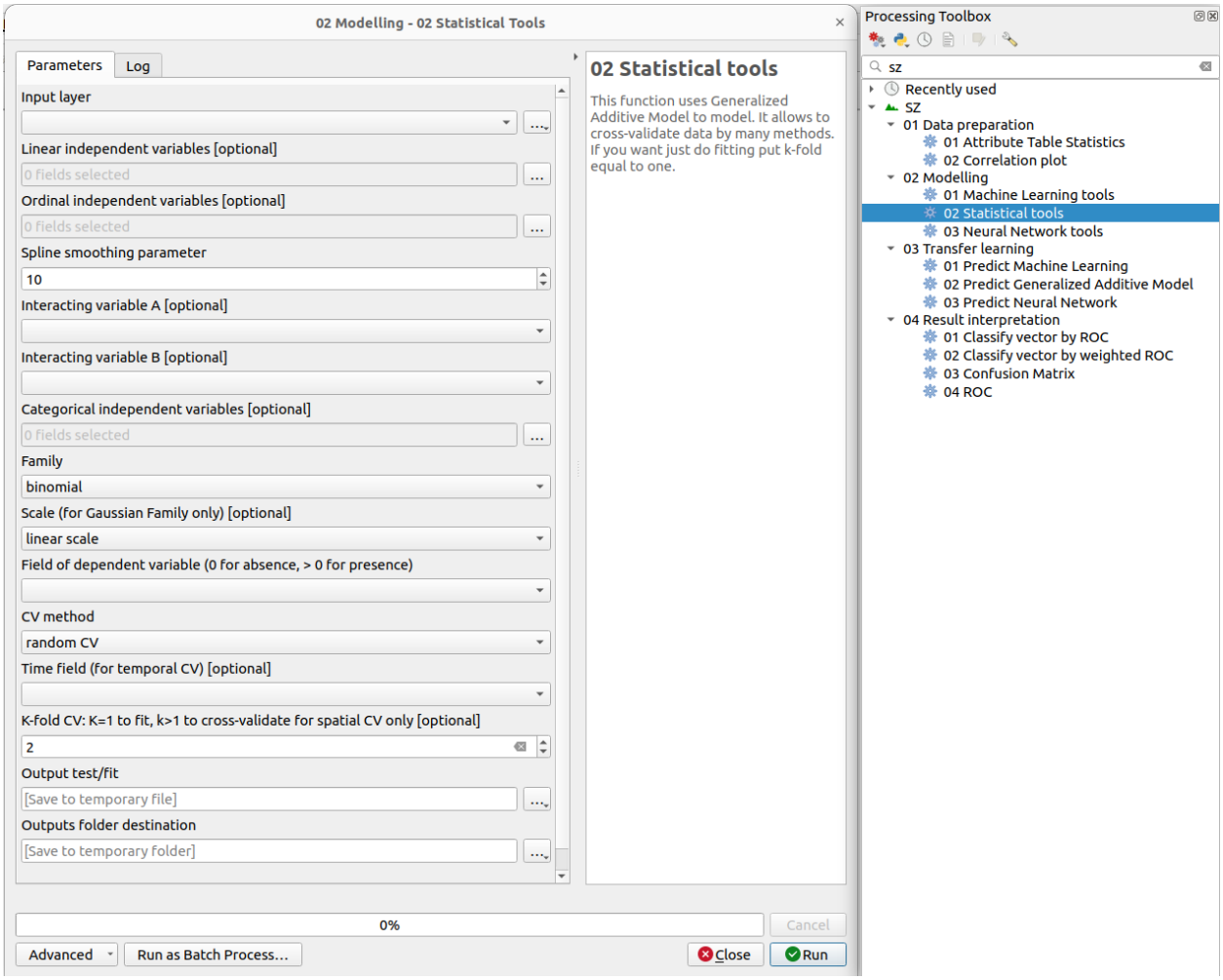

Figure 10: Screenshot of the plugin GUI, selecting the GAM mode as an example.

Whether a given user would focus on classification or regression tasks or whether this would be framed in a GAM or an MLP approach, all can be controlled in a few clicks. The interesting part to highlight here is that no input/output operations are needed, as all data

management requirements are taken care of by QGIS while modeling aspects are tasked to the Python script running in the background. The latter consideration is particularly relevant for stressing certain pros and cons of our plugin. For instance, as Python has essentially become the language of machine learning, the number of possibilities and future plugin releases is almost limitless. We certainly envision including tools belonging to deep learning that touch upon speech recognition (Fang et al., 2023; Nava et al., 2023) for time series analyses and even transformer neural networks (Dahal et al., 2024a; Lv et al., 2023) to potentially support large language models in the context of geospatial modeling (e.g., Fulman et al., 2024).

A limitation to consider is that the main efforts for the plugin development have been focused on two aspects. The first has been programming all space-time modeling modes and the cross-validation routines. The second focused on the interface. No efforts have been made to develop the native model architectures, which are called from already existing packages. This comes with the limitations specific to the package itself. For instance, the library behind the binomial and Gaussian GAM is *pygam* (Servén and Brummitt, 2018). This is one of the most powerful GAM inference tools among the available open implementations, but it does not have all the capabilities of the *mgcv* library (Wood, 2011) in R, from which it was inspired. For instance, *mgcv* allows for distributed calculation over multiple cores. Conversely, *pygam* only allows for serial computing.

As mentioned before, aside from different deep learning architectures, a possible improvement we envision is to extend the likelihoods beyond the binomial and Gaussian case to offer probability distributions typical of extreme value theory (Davison and Huser, 2015; Yadav et al., 2023). This could enable the plugin to be used for handling weather data formats typical of GIS platforms with ease, while also offering the ability to model extreme precipitation (Castro-Camilo and Huser, 2020) or temperature (Zhong et al., 2022) space-time patterns.

For reference to the reader, in a WINDOWS machine with 128 GB RAM and a processor Intel i9-14900K the MLP option run for calibration in 1 hour and 25 minutes, while with GAM option 8 minutes.

6 Conclusions

The power of GIS mainly resides in its data management capabilities and its wide reach among millions of practitioners worldwide, whether they work on landslides or any other spatio-temporal geospatial application typically associated to digital soil mapping, land use and tree species detection, etc.. Conversely, the power of data-driven models resides in their ability to look through past data to produce numerical expectations of what may happen. This is why the current version of the SZ-plugin tried to further extend the bridge connecting the two respective communities. Specifically, we have focused on enabling space-time modeling in the context of classification and regression. These two constitute fundamental aspects of most data-driven models, which can now be easily implemented alongside a full

suite of cross-validation routines and performance metrics. We have further allowed the two modeling modes to be run according to GAM or MLP options to highlight interpretable and performance-oriented considerations.

Future plugin releases will most likely be created to accommodate various likelihoods and spatiotemporal covariate effects that are still framed as part of GAMs. As for machine learning options, these will focus on allowing for different loss functions and extensions towards deep learning solutions.

To maximize the reach of and the support to the plugin, the SZ-plugin is now published in the QGIS official plugin list (plugins.qgis.org/plugins/sz_module), therefore it can be downloaded directly from QGIS. Moreover, the plugin is always accessible at the repository: github.com/SZtools/SZ-plugin, whereas its description and support can be found at the following website: sz-docs.readthedocs.io.

Our vision for this tool is to make complex models just a click away, even from those who may not have a formal data science background. Most importantly, even for those who may have such training, we hope to offer a drastic speed-up, removing the need for any I/O operation, and a standardized way of performing data analytics, model assessment and simulations, all from within QGIS.

7 Author contributions

Giacomo Titti: Conceptualization, Formal analysis, Software, Writing – original draft, Writing – review and editing. Liwei Hu: Formal analysis, Writing – original draft. Pietro Festi: Formal analysis, Writing – review and editing. Letizia Elia: Software, Writing – review and editing; Lisa Borgatti: Conceptualization, Writing – review and editing. Luigi Lombardo: Conceptualization, Formal analysis, Software, Writing – original draft, Writing – review and editing.

References

Ahmed, M., Tanyas, H., Huser, R., Dahal, A., Titti, G., Borgatti, L., Francioni, M. and Lombardo, L. (2023) Dynamic rainfall-induced landslide susceptibility: a step towards a unified forecasting system. International Journal of Applied Earth Observation and Geoinformation **125**, 103593.

Akgun, A., Sezer, E. A., Nefeslioglu, H. A., Gokceoglu, C. and Pradhan, B. (2012) An easy-to-use matlab program (mamland) for the assessment of landslide susceptibility using a mamdani fuzzy algorithm. Computers & Geosciences **38**(1), 23–34.

Alvioli, M., Marchesini, I., Reichenbach, P., Rossi, M., Ardizzone, F., Fiorucci, F. and Guzzetti, F. (2016) Automatic delineation of geomorphological slope units with r.slopeunits v1.0 and their optimization for landslide susceptibility modeling. Geoscientific Model Development **9**(11), 3975–3991.

Barna, D. M., Engeland, K., Kneib, T., Thorarinsdottir, T. L. and Xu, C.-Y. (2023) Regional index flood estimation at multiple durations with generalized additive models. EGUsphere **2023**, 1–43.

Basheer, M. and Oommen, T. (2024) Pylandslide: A python tool for landslide susceptibility mapping and uncertainty analysis. Environmental Modelling & Software **177**, 106055.

Ben-David, A. (2008) About the relationship between roc curves and cohen's kappa. Engineering Applications of Artificial Intelligence **21**(6), 874–882.

Brabb, E., Pampeyan, H. and Bonilla, M. (1972) MG 1972. landslide susceptibility in San Mateo County, California. US Geological Survey Miscellaneous Field Studies Map MF-360, scale **1**(62,500).

Bragagnolo, L., da Silva, R. V. and Grzybowski, J. M. V. (2020) Landslide susceptibility mapping with r. landslide: A free open-source gis-integrated tool based on artificial neural networks. Environmental Modelling & Software **123**, 104565.

Bryce, E., Lombardo, L., van Westen, C., Tanyas, H. and Castro-Camilo, D. (2022) Unified landslide hazard assessment using hurdle models: a case study in the island of dominica. Stochastic Environmental Research and Risk Assessment **36**(8), 2071–2084.

Castro-Camilo, D. and Huser, R. (2020) Local likelihood estimation of complex tail dependence structures, applied to us precipitation extremes. Journal of the American Statistical Association **115**(531), 1037–1054.

Chai, T. and Draxler, R. R. (2014) Root mean square error (rmse) or mean absolute error (mae)?–arguments against avoiding rmse in the literature. Geoscientific model development **7**(3), 1247–1250.

Chicco, D., Warrens, M. J. and Jurman, G. (2021) The coefficient of determination r-squared is more informative than smape, mae, mape, mse and rmse in regression analysis evaluation. Peerj computer science **7**, e623.

Crawley, M. J. (2012) The R book. John Wiley & Sons.

Dahal, A., Tanyaş, H. and Lombardo, L. (2024a) Full seismic waveform analysis combined with transformer neural networks improves coseismic landslide prediction. Communications Earth & Environment **5**(1), 75.

Dahal, A., Tanyas, H., van Westen, C., van der Meijde, M., Mai, P. M., Huser, R. and Lombardo, L. (2024b) Space–time landslide hazard modeling via ensemble neural networks. Natural Hazards and Earth System Sciences **24**(3), 823–845.

Davison, A. C. and Huser, R. (2015) Statistics of extremes. Annual Review of Statistics and its Application **2**, 203–235.

De Myttenaere, A., Golden, B., Le Grand, B. and Rossi, F. (2016) Mean absolute percentage error for regression models. Neurocomputing **192**, 38–48.

Eaton, J. W., Bateman, D., Hauberg, S. et al. (1997) Gnu octave. Network thoery London.

Elia, L., Castellaro, S., Dahal, A. and Lombardo, L. (2023) Assessing multi-hazard susceptibility to cryospheric hazards: Lesson learnt from an alaskan example. Science of the Total Environment **898**, 165289.

Fang, Z., Tanyas, H., Gorum, T., Dahal, A., Wang, Y. and Lombardo, L. (2023) Speech-recognition in landslide predictive modelling: A case for a next generation early warning system. Environmental Modelling & Software **170**, 105833.

Fang, Z., Wang, Y., van Westen, C. and Lombardo, L. (2024a) Landslide hazard spatiotemporal prediction based on data-driven models: Estimating where, when and how large landslide may be. International Journal of Applied Earth Observation and Geoinformation **126**, 103631.

Fang, Z., Wang, Y., van Westen, C. and Lombardo, L. (2024b) Space–time landslide susceptibility modeling based on data-driven methods. Mathematical Geosciences **56**(6), 1335–1354.

Fell, R., Corominas, J., Bonnard, C., Cascini, L., Leroi, E., Savage, W. Z. et al. (2008) Guidelines for landslide susceptibility, hazard and risk zoning for land-use planning. Engineering Geology **102**(3-4), 99–111.

Flenniken, J. M., Stuglik, S. and Iannone, B. V. (2020) Quantum gis (qgis): An introduction to a free alternative to more costly gis platforms: For359/fr428, 2/2020. Edis **2020**(2), 7–7.

Forte, G., Verrucci, L., Di Giulio, A., De Falco, M., Tommasi, P., Lanzo, G., Franke, K. W. and Santo, A. (2021) Analysis of major rock slides that occurred during the 2016–2017 central italy seismic sequence. Engineering Geology **290**, 106194.

Fulman, N., Memduhoğlu, A. and Zipf, A. (2024) Distortions in judged spatial relations in large language models. The Professional Geographer pp. 1–9.

Guzzetti, F., Carrara, A., Cardinali, M. and Reichenbach, P. (1999) Landslide hazard evaluation: A review of current techniques and their application in a multi-scale study, central italy. Geomorphology **31**(1), 181–216.

Hinton, G. E. (1989) Connectionist learning procedures. Artificial Intelligence **40**, 185–234.

Hodson, T. O. (2022) Root mean square error (rmse) or mean absolute error (mae): When to use them or not. Geoscientific Model Development Discussions **2022**, 1–10.

Hosmer, D. W. and Lemeshow, S. (2000) Applied Logistic Regression. Second edition. New York: Wiley.

LeCun, Y., Bengio, Y. and Hinton, G. E. (2015) Deep learning. Nature **521**, 436–444.

Lee, C., Huang, C., Tsao, T., Wei, L., Huang, W., Cheng, C. and Chi, C. (2016) Combining rainfall parameter and landslide susceptibility to forecast shallow landslide in taiwan. Geotechnical Engineering Journal of the SEAGS & AGSSEA **47**(2), 72–82.

Loche, M. and Scaringi, G. (2023) Temperature and shear-rate effects in two pure clays: Possible implications for clay landslides. Results in Engineering **20**, 101647.

Loche, M., Scaringi, G., Yunus, A. P., Catani, F., Tanyaş, H., Frodella, W., Fan, X. and Lombardo, L. (2022) Surface temperature controls the pattern of post-earthquake landslide activity. Scientific reports **12**(1), 988.

Lombardo, L., Opitz, T., Ardizzone, F., Guzzetti, F. and Huser, R. (2020) Space-time landslide predictive modelling. Earth-Science Reviews p. 103318.

Lombardo, L., Tanyas, H., Huser, R., Guzzetti, F. and Castro-Camilo, D. (2021) Landslide size matters: A new data-driven, spatial prototype. Engineering Geology **293**, 106288.

Lv, P., Ma, L., Li, Q. and Du, F. (2023) Shapeformer: A shape-enhanced vision transformer model for optical remote sensing image landslide detection. IEEE Journal of Selected Topics in Applied Earth Observations and Remote Sensing **16**, 2681–2689.

Melis, M. T., Da Pelo, S., Erbì, I., Loche, M., Deiana, G., Demurtas, V., Meloni, M. A., Dessì, F., Funedda, A., Scaioni, M. et al. (2020) Thermal remote sensing from uavs: A review on methods in coastal cliffs prone to landslides. Remote Sensing **12**(12), 1971.

Millington, J. D. (2005) Wildfire risk mapping: considering environmental change in space and time. Journal of Mediterranean ecology **6**(1/4), 33.

Moreno, M., Lombardo, L., Crespi, A., Zellner, P. J., Mair, V., Pittore, M., van Westen, C. and Steger, S. (2024) Space-time data-driven modeling of precipitation-induced shallow landslides in south tyrol, italy. Science of the Total Environment **912**, 169166.

Nava, L., Carraro, E., Reyes-Carmona, C., Puliero, S., Bhuyan, K., Rosi, A., Monserrat, O., Floris, M., Meena, S. R., Galve, J. P. et al. (2023) Landslide displacement forecasting using deep learning and monitoring data across selected sites. Landslides **20**(10), 2111–2129.

Opitz, T., Bakka, H., Huser, R. and Lombardo, L. (2022) High-resolution bayesian mapping of landslide hazard with unobserved trigger event. The Annals of Applied Statistics **16**(3), 1653–1675.

Osna, T., Sezer, E. A. and Akgun, A. (2014) Geofis: an integrated tool for the assessment of landslide susceptibility. Computers & Geosciences **66**, 20–30.

Ray, R. L., Jacobs, J. M. and Cosh, M. H. (2010) Landslide susceptibility mapping using downscaled amsr-e soil moisture: A case study from cleveland corral, california, us. Remote sensing of environment **114**(11), 2624–2636.

Reichenbach, P., Mondini, A., Rossi, M. et al. (2014) The influence of land use change on landslide susceptibility zonation: the Briga catchment test site (Messina, Italy). Environmental management **54**(6), 1372–1384.

Reichenbach, P., Rossi, M., Malamud, B. D., Mihir, M. and Guzzetti, F. (2018) A review of statistically-based landslide susceptibility models. Earth-Science Reviews **180**, 60–91.

Rossi, M. and Reichenbach, P. (2016) LAND-SE: a software for statistically based landslide susceptibility zonation, version 1.0. Geoscientific Model Development **9**(10), 3533.

Rumelhart, D. E., Hinton, G. E. and Williams, R. J. (1986) Learning representations by back-propagating errors. Nature **323**, 533–536.

Sahin, E. K., Colkesen, I., Acmali, S. S., Akgun, A. and Aydinoglu, A. C. (2020) Developing comprehensive geocomputation tools for landslide susceptibility mapping: Lsm tool pack. Computers & geosciences **144**, 104592.

Samia, J., Temme, A. J., Bregt, A., Wallinga, J., Fausto Guzzetti, Ardizzone, F. and Rossi, M. (2017a) Characterization and quantification of path dependency in landslide susceptibility. Geomorphology **292**, 16–24.

Samia, J., Temme, A. J., Bregt, A., Wallinga, J., Guzzetti, F., Ardizzone, F. and Rossi, M. (2017b) Do Landslides Follow Landslides? Insights in Path Dependency from a Multi-Temporal Landslide Inventory. Landslides **14**, 547–558.

Schober, P., Boer, C. and Schwarte, L. A. (2018) Correlation coefficients: appropriate use and interpretation. Anesthesia & analgesia **126**(5), 1763–1768.

Segoni, S., Lagomarsino, D., Fanti, R., Moretti, S. and Casagli, N. (2015) Integration of rainfall thresholds and susceptibility maps in the emilia romagna (italy) regional-scale landslide warning system. Landslides **12**, 773–785.

Segoni, S., Piciullo, L. and Gariano, S. L. (2018a) A review of the recent literature on rainfall thresholds for landslide occurrence. Landslides **15**(8), 1483–1501.

Segoni, S., Tofani, V., Rosi, A., Catani, F. and Casagli, N. (2018b) Combination of rainfall thresholds and susceptibility maps for dynamic landslide hazard assessment at regional scale. Frontiers in Earth Science **6**, 85.

Servén, D. and Brummitt, C. (2018) pygam: Generalized additive models in python. Zenodo. doi **10**.

Sezer, E. A., Nefeslioglu, H. A. and Osna, T. (2017) An expert-based landslide susceptibility mapping (lsm) module developed for netcad architect software. Computers & Geosciences **98**, 26–37.

Sokolova, M., Japkowicz, N. and Szpakowicz, S. (2006) Beyond accuracy, f-score and roc: a family of discriminant measures for performance evaluation. In Australasian joint conference on artificial intelligence, pp. 1015–1021.

Steger, S. and Glade, T. (2017) The challenge of "trivial areas" in statistical landslide susceptibility modelling. In Advancing Culture of Living with Landslides: Volume 2 Advances in Landslide Science, pp. 803–808.

Steger, S. and Kofler, C. (2019) Statistical modeling of landslides: landslide susceptibility and beyond. In Spatial Modeling in GIS and R for Earth and Environmental Sciences, pp. 519–546. Elsevier.

Steger, S., Moreno, M., Crespi, A., Gariano, S. L., Brunetti, M. T., Melillo, M., Peruccacci, S., Marra, F., de Vugt, L., Zieher, T. et al. (2024) Adopting the margin of stability for space–time landslide prediction–a data-driven approach for generating spatial dynamic thresholds. Geoscience Frontiers **15**(5), 101822.

Steger, S., Moreno, M., Crespi, A., Zellner, P. J., Gariano, S. L., Brunetti, M. T., Melillo, M., Peruccacci, S., Marra, F., Kohrs, R. et al. (2023) Deciphering seasonal effects of triggering and preparatory precipitation for improved shallow landslide prediction using generalized additive mixed models. Natural Hazards and Earth System Sciences **23**(4), 1483–1506.

Tanyaş, H., Görüm, T., Kirschbaum, D. and Lombardo, L. (2022) Could road constructions be more hazardous than an earthquake in terms of mass movement? Natural hazards **112**(1), 639–663.

Titti, G., Antelmi, M., Fusco, F., Longoni, L., Borgatti, L. et al. (2024) A new perspective for regional landslide susceptibility assessment. Italian journal of engineering geology and environment **1**(Special Issue 1), 275–283.

Titti, G., Sarretta, A., Lombardo, L., Crema, S., Pasuto, A. and Borgatti, L. (2022) Mapping susceptibility with open-source tools: a new plugin for qgis. Frontiers in Earth Science **10**, 842425.

Torizin, J., Schüssler, N. and Fuchs, M. (2022) Landslide susceptibility assessment tools v1. 0.0 b–project manager suite: a new modular toolkit for landslide susceptibility assessment. Geoscientific Model Development **15**(7), 2791–2812.

Van Rossum, G. et al. (2007) Python programming language. In USENIX annual technical conference, volume 41, pp. 1–36.

Varnes and the IAEG Commission on Landslides and Other Mass-Movements (1984) Landslide hazard zonation: A review of principles and practice. Natural Hazards, Series. Paris: United Nations Economic, Scientific and cultural organization. UNESCO **3**, 63.

Wang, N., Cheng, W., Marconcini, M., Bachofer, F., Liu, C., Xiong, J. and Lombardo, L. (2022) Space-time susceptibility modeling of hydro-morphological processes at the Chinese national scale. Engineering geology **301**, 106586.

Wang, T., Dahal, A., Fang, Z., van Westen, C., Yin, K. and Lombardo, L. (2024) From spatio-temporal landslide susceptibility to landslide risk forecast. Geoscience Frontiers **15**(2), 101765.

Wood, S. N. (2004) Stable and efficient multiple smoothing parameter estimation for generalized additive models. Journal of the American Statistical Association **99**(467), 673–686.

Wood, S. N. (2011) Fast stable restricted maximum likelihood and marginal likelihood estimation of semiparametric generalized linear models. Journal of the Royal Statistical Society (B) **73**(1), 3–36.

Yadav, R., Huser, R., Opitz, T. and Lombardo, L. (2023) Joint modelling of landslide counts and sizes using spatial marked point processes with sub-asymptotic mark distributions. Journal of the Royal Statistical Society Series C: Applied Statistics **72**(5), 1139–1161.

Zhong, P., Huser, R. and Opitz, T. (2022) Modeling nonstationary temperature maxima based on extremal dependence changing with event magnitude. The Annals of Applied Statistics **16**(1), 272–299.